Neutron inelastic scattering measurements on ^{136}Xe at $E_n = 0.7$ to 100 MeV

S. J. Daugherty,* J. B. Albert, and L. J. Kaufman†
Physics Department and CEEM, Indiana University, Bloomington, Indiana 47405, USA

M. Devlin, N. Fotiades, and R. O. Nelson
Los Alamos National Laboratory, Los Alamos, New Mexico 87545, USA

M. Krtička
Faculty of Mathematics and Physics, Charles University, CZ-180 00 Prague, Czech Republic

(Received 16 July 2018; published 10 December 2018)

Experiments searching for neutrinoless double β decay ($0\nu\beta\beta$) require precise energy calibration and extremely low backgrounds. One of the most popular isotopes for $0\nu\beta\beta$ experiments is ^{136}Xe. In support of these experiments, the neutron inelastic scattering properties of this isotope have been measured at the GErmanium Array for Neutron Induced Excitations (GEANIE) at the Los Alamos Neutron Science Center. Time-of-flight techniques are utilized with high-purity germanium detectors to search for inelastic scattering γ rays for neutron energies between 0.7 and 100 MeV. Limits are set on production of yet-unobserved γ rays in the energy range critical for $0\nu\beta\beta$ studies, and measurements are made of multiple γ-ray production cross sections. In particular, we have measured the production of the 1313 keV γ ray, which comes from the transition of the first-excited to ground state of ^{136}Xe. This neutron-induced γ line may be useful for a novel energy calibration technique, described in this paper.

DOI: 10.1103/PhysRevC.98.064606

I. INTRODUCTION

Neutrinoless double β decay ($0\nu\beta\beta$) is a hypothetical lepton-number-violating decay mode of great interest to nuclear and particle physics. Its observation would confirm that neutrinos are Majorana particles, meaning there is no distinction between neutrinos and antineutrinos. Measurement of this process could, in the Majorana neutrino case, also be used to infer the absolute mass of the neutrino. Given the interest in these neutrino properties, several experimental collaborations are running or developing experiments to search for $0\nu\beta\beta$.

One of the most popular and successful isotopes for this search is ^{136}Xe [1–6]. This isotope has several advantages, including the large Q value (2457.83 keV [7]), ease of enrichment and purification, and physical characteristics allowing for scaling to large monolithic detectors. While the signal for $0\nu\beta\beta$ is a spatially compact monoenergetic peak at the Q value, signals detected at other energies and with spatially separated (multisite) energy deposits can be used to identify and constrain backgrounds. Proposed next-generation experiments (such as nEXO [1]) will have reduced radiogenic backgrounds (such as the 2448 keV line from ^{214}Bi decay) due to purification, high-radiopurity shielding, topological discrimination, and other techniques. With these backgrounds mitigated, less common backgrounds will become more prominent. Current and future experiments using ^{136}Xe (including nEXO, NEXT [5], PandaX-III [6], and KamLAND-Zen [4]) will benefit from having the best possible understanding of all potential backgrounds.

As such, we have measured the production of γ rays in ^{136}Xe from fast neutron interactions. This complements previous work [8] studying γ rays from neutron capture on ^{136}Xe. While neutron-induced γ rays are not expected to be a significant background in future deep underground detectors, a detailed understanding of them may help identify otherwise mysterious signals. Cross sections as a function of neutron energy have been measured for several of the major γ-ray energies, and limits have been set on the potential cross sections of unknown γ lines, which might mimic a $0\nu\beta\beta$ signal. The measured cross sections for γ lines produced in fast neutron-induced reactions may be used to refine future nuclear evaluations and improve simulations of the reactions.

This work also suggests a novel method for detector energy calibration. The 1313 keV level of ^{136}Xe is the first-excited state, and can be reached through neutron inelastic scattering (n, n'). Thus, fast neutrons could be produced and sent into the detector to excite ^{136}Xe nuclei to this state, causing them to emit this monoenergetic γ line, offering a calibration signal.

II. EXPERIMENTAL SETUP

Data were collected at the Los Alamos Neutron Science Center (LANSCE) Weapons Neutron Research (WNR) facility [9]. There, an 800-MeV proton beam incident on a natural

*seajdaug@indiana.edu
†Also at SLAC National Accelerator Laboratory, Menlo Park, California, USA.

 ©2018 American Physical Society

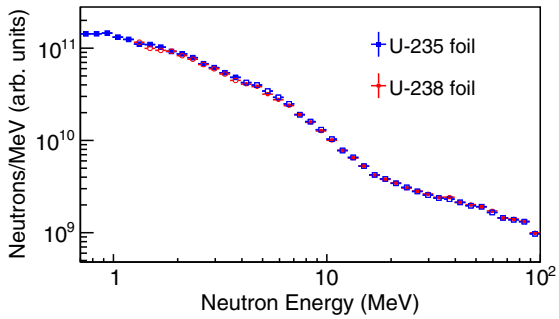

FIG. 1. Measured neutron flux spectrum at GEANIE. The relative flux magnitudes for the xenon and iron calibration data sets were determined exclusively using the ^{235}U fission foil data, as the ^{238}U efficiency was less stable. This figure is not normalized to any specific set of beam time. The flux shape was determined by the ^{235}U (^{238}U) data for $E_n \leqslant 4$ MeV ($E_n > 4$ MeV). Open markers are used here to demonstrate flux shape agreement between the two measurements.

tungsten target produces neutrons in a wide energy range. The proton beam is delivered in short pulses spaced 1.8μs apart (micropulses), in groups lasting for 625 μs (macropulses). There are 100 macropulses per second.

Our sample of 99.925% enriched ^{136}Xe was contained in a thin cylindrical aluminum vessel with thin kapton windows for neutrons to pass through. The target vessel window diameter of 3.4 cm is larger than the measured beam diameter, so the precise beam profile is not relevant to the cross-section measurement. The vessel was pressurized to near 2700 torr absolute, with pressure monitored in real time using a capacitance manometer to account for changes due to temperature and a very slow leak. The xenon volume is 7.2 cm long and 3.4 cm diameter, located on flight path 60R of the WNR neutron beam, centered 20.34 m downstream of the proton target, in the center of the GErmanium Array for Neutron Induced Excitations (GEANIE) spectrometer [10].

GEANIE features an array of 20 Compton-suppressed high-purity germanium (HPGe) detectors to detect neutron-induced γ rays. Neutron energy is determined via time of flight. Neutron flux is measured by a fission chamber in the beam line upstream from the target with ^{235}U and ^{238}U foils [11]. Figure 1 shows the measured neutron flux as a function of neutron energy. More details on GEANIE, the WNR beam, and the procedures for cross-section measurement can be found in other papers [12–15].

III. DATA ANALYSIS

A. Absolute cross sections

To minimize uncertainties due to absolute detector efficiency and neutron flux, we normalized our xenon cross-section measurements to a reference ^{56}Fe cross section. To do so, we added 50 μm thick natural iron foils to the ends of the target vessel for certain runs. Our reference cross section was 1.5 ± 0.1 b for production of the 847 keV γ in ^{56}Fe at $E_n = 6.2$ MeV, taken from a measurement by Beyer *et al.* [16] at the nELBE photoneutron source. This γ line is the transition from the first-excited to ground state of ^{56}Fe. We corrected this cross section for small angular variations using angular coefficients from another measurement at nELBE, by Dietz *et al.* [17]. After corrections for detector live-time, this line provided a reliable calibration for measurement of the absolute cross section. Our vessel was filled with nitrogen during most of the iron foil calibration runs to keep neutron scattering rates similar to xenon while avoiding any possible interference due to the 847 keV γ rays emitted from ^{134}Xe produced via $(n, 3n)$ interactions. We also took some iron foil data with the vessel filled with xenon to confirm the validity of our analysis. Lastly, runs with the target vessel filled with nitrogen (both with and without iron foils) were used to identify backgrounds not due to neutron interactions on xenon.

The relative detector efficiencies at different γ energies were determined using a ^{152}Eu source placed at the center of the detector array. This provided γ rays with known relative intensities between 444 and 1299 keV. We determined an efficiency curve by fitting the data with [18]

$$\log(\epsilon_\gamma) = a + b\log(E_\gamma) + c\log^2(E_\gamma). \quad (1)$$

Successful extrapolation of this efficiency curve to higher γ-ray energies has been demonstrated in previous GEANIE measurements [14,19]. The known ^{152}Eu lines, along with some higher-energy lines from (n, n') interactions on ^{136}Xe, were also used to calibrate the conversion from ADC counts to measured γ-ray energy.

The GEANIE spectrometer includes both coaxial and planar HPGe detectors, though we utilized only the coaxial ones. The planar detectors can only measure γ rays up to 1 MeV, well below the energies of interest to $0\nu\beta\beta$ experiments. Some of the coaxial detectors showed poor performance in neutron or γ energy reconstruction, possibly due to neutron damage, and were excluded from the analysis, leaving five detectors with usable data.

A simple Gaussian-plus-linear fit is performed for each bin in E_n for each γ peak to define the integration range in each of the HPGe detectors used. The γ yield is then determined by summing counts in the peak range of $\pm 3.5\sigma$ and subtracting the background (estimated as the linear part of the fit). Figure 2 shows example γ spectra and an example fit. Live-time fractions for the fission chambers and HPGe detectors are determined for each run by comparing ADC triggers with dead-time free scaler counts. The measured yields, live-times, efficiencies, and γ-ray attenuation corrections are combined similarly to the method described in Ref. [12] to determine partial γ-ray cross sections. Our analysis differs in that we normalize to an iron cross section, rather than lead, and that we neglect internal conversion coefficients, looking only at γ production. The influence of internal conversion is very weak (much smaller than measurement uncertainties) for all measured γ rays [20].

Our analysis also differs in the method of dealing with anisotropic γ emission. The neutron-induced γ emission will not be isotropic, but rather will have some angular distribution, which may be, for known spin states, estimated. The estimation of these angular distributions is nontrivial, and we

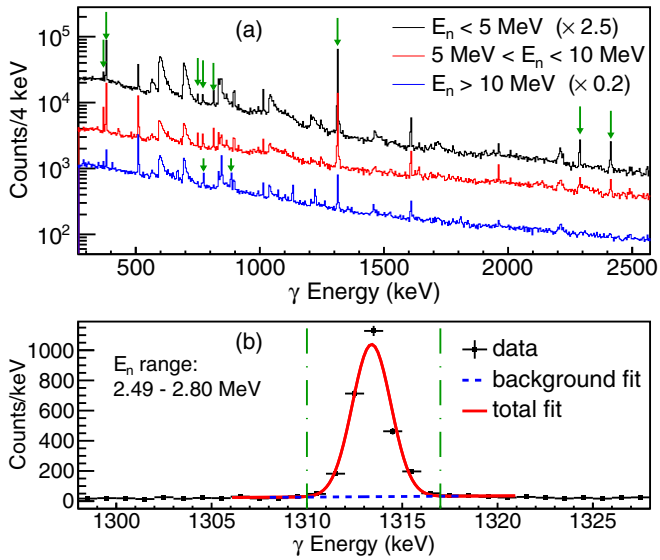

FIG. 2. (a) Spectra of γ rays detected by one of the HPGe detectors. Three different neutron energy ranges are shown: $E_n <$ 5 MeV (top), 5 MeV $< E_n <$ 10 MeV (middle), and $E_n >$ 10 MeV (bottom). The top (bottom) curve has been scaled by a factor of 2.5 (0.2) to make it easier to distinguish the spectra. Downward pointing arrows indicate the peaks for which we have determined cross sections in this work. Other peaks visible in this figure are also present in data taken without xenon in the target vessel, and thus are considered to be background lines. (b) A fit to the 1313 keV line, for a single bin in E_n. The vertical axis gives the detected counts in a single detector. The solid and dashed lines show the total fit and background contribution, respectively, and the vertical broken lines indicate the boundaries of the integration window for the peak.

chose instead to minimize the angular effects where possible, and accept a larger uncertainty elsewhere. We model the angular correction, as is typical, with

$$C_\gamma(E_n,\theta) = \frac{1}{W(E_n,\theta)}; \tag{2}$$

$$W(E_n,\theta) = 1 + A_2P_2(\cos\theta) + A_4P_4(\cos\theta), \tag{3}$$

where A_k are coefficients and P_k are the Legendre polynomials [17]. With cross-section measurements at three distinct $|\cos\theta|$ values, it is possible to add the three measurements linearly with coefficients β_i for different detectors i such that the deviations from $C_\gamma(E_n,\theta) = 1$ will cancel out, regardless of the A_k coefficients. This calculation uses the approximation $1/(1+x) \approx 1 - x$ for small $x = A_2P_2 + A_4P_4$, and is accurate to order x^2. Among our five detectors, we have three detectors at nearly the same value of $|\cos\theta|$, and two others at sufficiently different values. Unfortunately, one of the detectors at a unique angle was unable to record γ rays above 2 MeV, so this cancellation only works below $E_\gamma =$ 2 MeV. Above that energy, uncertainties are higher due to both angular correction uncertainties as well as larger uncertainties on the absolute detector efficiency. For all γ lines below 2 MeV, the measured cross sections from individual detectors i are added together with appropriate coefficients β_i to cancel out anisotropic effects. Above $E_\gamma = 2$ MeV, the four detectors simply have their measured cross sections averaged, so $\beta_i =$ 0.25. Our final cross section is then given as the weighted sum of that from individual detectors after normalization to the iron measurement,

$$\sigma_\gamma(E_n) = \sum_i \beta_i \sigma_{\gamma,i}(E_n). \tag{4}$$

TABLE I. Evaluated systematic uncertainties for cross-section measurements. Xenon angular effects dominate the systematic uncertainty for $E_\gamma > 2$ MeV, where cancellation was impossible. These relative uncertainties are uncorrelated, and are added in quadrature.

Source	Uncertainty
reference σ_{Fe}	6.7%
σ_{Fe} angular correction	7.9%
iron thickness	2%
iron/xenon efficiency difference	4%
γ ray attenuation	3%
HPGe detector $\epsilon(\gamma)$ ($E_\gamma < 2$ MeV)	3%
HPGe detector $\epsilon(\gamma)$ ($E_\gamma > 2$ MeV)	6%
xenon thickness	3.3%
xenon angular effects ($E_\gamma < 2$ MeV)	3%
xenon angular effects ($E_\gamma > 2$ MeV)	18%

B. Systematic uncertainties

Table I summarizes the cross-section measurement systematic uncertainties. By design, large uncertainties associated with absolute detector efficiency and absolute neutron flux are canceled by the iron normalization. Thus, for $E_n < 2$ MeV, the systematic uncertainty is dominated by the precision of the reference iron cross-section measurements. We chose to treat discrepancies in angular-correction measurements between different detectors from Ref. [17] as an angular uncertainty, making the iron angular distribution a leading uncertainty term.

Angular-distribution uncertainties for xenon were estimated by assuming that the xenon anisotropy should be similar to that of iron [17] or lead [12], and using the largest anisotropy factors as a conservative estimate. Variations in measured xenon cross sections between individual HPGe detectors at different angles are consistent with or smaller than the 18% deviations found in other measurements, so this uncertainty is appropriate. For $E_\gamma < 2$ MeV, this anisotropy is largely canceled as described in Sec. III A, giving a smaller uncertainty.

Attenuation corrections were calculated using MCNPX [21], and the corrections are conservatively treated also as an uncertainty. The geometric efficiency differences between xenon and iron were computed with a simple custom Monte Carlo simulation, and are kept small by the use of multiple detectors at different angles. Detector γ-efficiency uncertainty is based on the efficiency fit to the ^{152}Eu data. An additional uncertainty is added above 2 MeV to account for deviations in the efficiency curve extrapolation [14,19,22]. Xenon-thickness uncertainty comes from temperature uncertainty, changing xenon pressure, and a slight ballooning of the kapton windows at the ends of the target vessel.

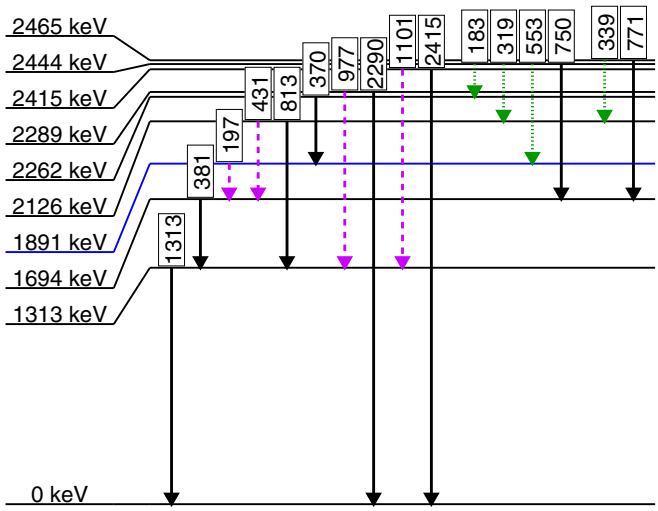

FIG. 3. Diagram of levels up to 2500 keV, and their transitions, for ^{136}Xe. Level scheme is taken from Ref. [23]. Energies are in keV. Transitions with solid lines have cross sections determined in this work. Dashed lines indicate that the transitions were observed, but could not have cross sections precisely determined due to an interfering background line, low statistics, or other issue. Dotted lines indicate that the γ yield from those transitions was too weak to be clearly identified. The 1891 keV level is notable for its long half-life of nearly 3μs.

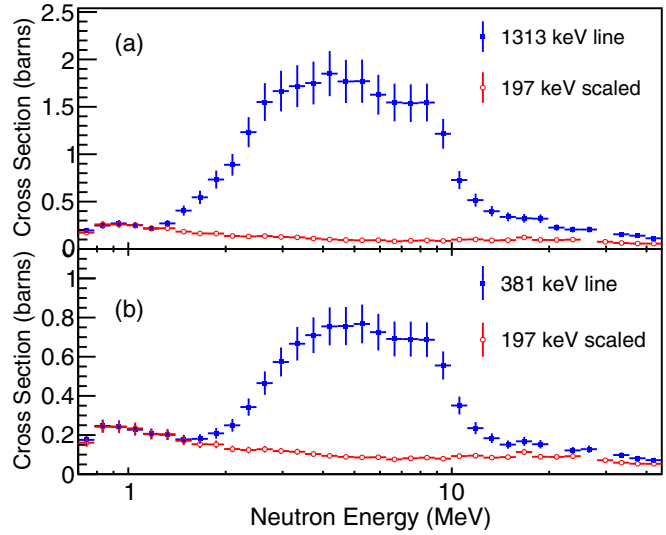

FIG. 4. Unsubtracted cross sections for the 1313 keV (a) and 381 keV (b) lines, along with a scaled cross section for the 197 keV line. The agreement of the cross section shape with time-of-flight corresponding to energies below $E_n = 1.3$ MeV suggests that the observed events below threshold are due entirely to the metastable state at 197 keV. The final cross-section evaluation (Fig. 5) has the scaled 197 keV cross section subtracted off, leaving only prompt γ emission. Error bars here include both statistical and systematic effects.

C. Metastable state

Figure 3 shows the level diagram for ^{136}Xe, with levels up to 2500 keV. Notably, the 1891 keV level is much longer lived than the others, with a nearly 3 μs half-life [23]. This metastable state interferes with the time-of-flight measurement of E_n. As a result, the 197 keV γ-emission cross section cannot be properly measured, and there is a delayed component to the 1313 keV and 381 keV lines that interferes. We subtract off the delayed component of these lines (which has the same time-of-flight distribution as the 197 keV line) to leave only prompt γ emission. Figure 4 shows this subtraction for both these lines. While the full cross section for this delayed emission cannot be precisely determined, we estimate from our measurements that 28% (12%) of emission is delayed for the 381 keV (1313 keV) line.

IV. INELASTIC SCATTERING MEASUREMENTS

Cross sections could only be determined for γ lines with sufficient yield to be fit successfully in all available detectors, and only if a γ ray of similar intensity and energy is not present in background. After these selections, we are left with eight lines from (n, n') interactions. These measured cross sections are shown in Fig. 5 and Fig. 6, along with estimates from TALYS 1.8 [24]. Several other γ lines were observed, with most of them identified as being due to (n, xn) interactions for $x = 2, 3, 4, 5$. Most of these either had low statistics or an interfering background, and so a full cross-section determination was not possible. The cross section for one line each from $(n, 3n)$ and $(n, 5n)$ could be determined, and are shown in Fig. 7. In these figures, bins in E_n with no marker do not necessarily indicate zero cross section, but may be bins where, due to low statistics, the peak fit for data from one or more detectors failed. Lines at 1640, 1690, and 2009 keV appeared for $E_n < 5$ MeV and were identified as likely being from ^{136}Xe(n, n'), though were not measurable due to interfering nearby lines or low statistics. These lines do not correspond to any obvious known transition in the ENSDF database [25]. Another unknown line at 1355 keV was seen, though it only appeared with $E_n > 10$ MeV, and is likely an unknown line from some daughter nucleus of a neutron-induced reaction.

V. LIMITS ON NEW γ LINES RELEVANT TO $0\nu\beta\beta$

The discovery of a new γ line produced from neutron interactions on ^{136}Xe could be an important consideration for next-generation $0\nu\beta\beta$ experiments. As such, we have searched for γ peaks between 2350 and 2550 keV around the ^{136}Xe $0\nu\beta\beta$ Q value of 2457.8 keV [7]. The count spectra from the four HPGe detectors summed is shown in Fig. 8. For the calculation of cross-section limits, we use only data from one detector (systematic uncertainties are larger than statistical ones here). Limits are based on a sliding 5 keV E_γ window, in which counts above background are considered with Poisson statistics to determine a 90% upper limit on peak intensity. The rest of the cross-section determination and systematic uncertainties are as described in Sec. III.

There is a known line at 2415 keV from a transition to the ground state of ^{136}Xe. This is separated in energy from the Q value by 1.8%. Our measurements of this line are shown in Fig. 6(f). The rest of the spectrum is relatively flat, though

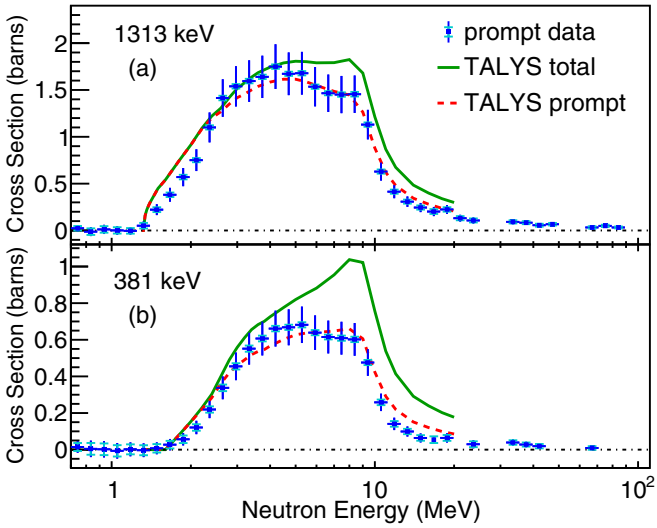

FIG. 5. Measured cross sections for the two dominant γ-ray production lines, (a) 1313 keV and (b) 381 keV, from (n, n'). Measured prompt γ-ray production cross sections are indicated with blue square markers and error bars, with delayed production subtracted out as described in Sec. III C. Blue (cyan) error bars here, and in subsequent figures, indicate combined statistical and systematic errors (statistical errors alone). The TALYS 1.8 prediction for total (prompt) γ-ray production is indicated with a solid green line (dashed red line).

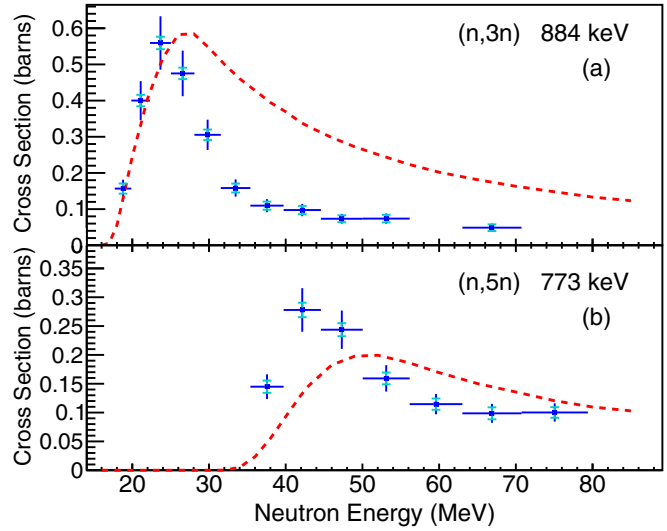

FIG. 7. Measured cross sections for γ-ray production from $(n, 3n)$ and $(n, 5n)$ interactions. Measured values are indicated with blue square markers and error bars, while TALYS 1.8 predictions are red dashed lines.

there is a small peak near 2491 keV, 1.4% away from the Q value. This peak is seen in all three E_n regions, and we determined cross section upper limits on this peak to be 13, 48, and 37 mb in the $E_n < 5$ MeV, 5 MeV $< E_n <$ 10 MeV, and $E_n > 10$ MeV ranges, respectively. Note that these limits are for cross sections averaged over the neutron energy range, weighted by the GEANIE flux. The source of this peak is unknown, but its energy matches a known transition in ^{72}Ge, and a search for this peak in our non-xenon data was inconclusive. No other new peaks of comparable magnitude were found near the ^{136}Xe Q value, so these cross-section limits hold for any new peaks in this γ-energy range.

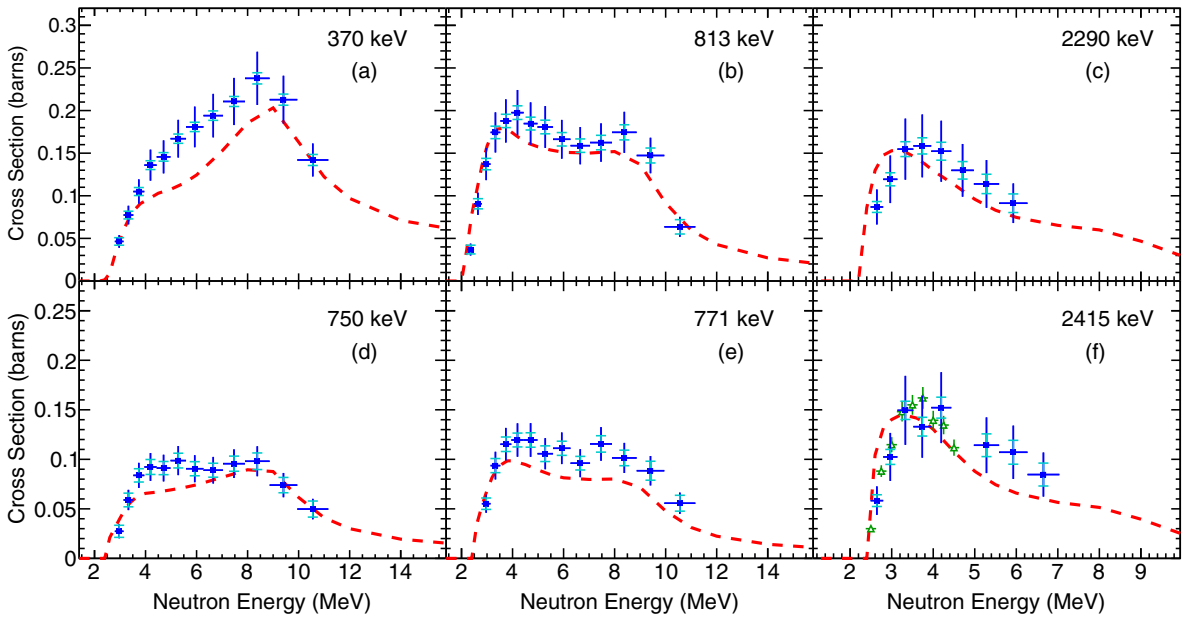

FIG. 6. Measured cross sections for γ-ray production from several (n, n') inelastic scattering interactions. Measured values are indicated with blue square markers and error bars, while TALYS 1.8 predictions are red dashed lines. (f) The 2415 keV measurement additionally is compared to recent results from Peters *et al.* [26], indicated by open green triangles.

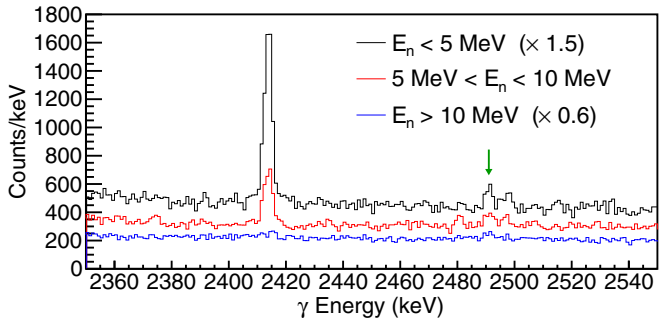

FIG. 8. Sum of detected counts in four HPGe detectors for E_γ in the general region of interest for ^{136}Xe $0\nu\beta\beta$ experiments. The spectra have been separated into three neutron energy ranges via scaling as they were in Fig. 2(a). A peak near 2491 keV (possibly due to inelastic scattering on the germanium detectors) is indicated with an arrow.

VI. NOVEL CALIBRATION TECHNIQUE

Neutron-induced excitation to the 1313 keV level is the primary γ-producing interaction observed for fast neutrons below ~2.5 MeV in energy. Thus, neutron inelastic scattering could potentially be a source of monoenergetic 1313 keV γ rays for calibration of a future $0\nu\beta\beta$ detector. A great strength of proposed experiments, such as nEXO [1], is the pure, monolithic, self-shielding, active detector volume. Without radioisotopes being introduced into the detector, very few γ rays will reach the central part of the xenon volume. This is excellent for background reduction, but potentially problematic for calibration.

It may be possible to use a DD (deuterium-deuterium) generator located outside the xenon volume to deliver 2.5 MeV neutrons deep into the detector, exciting ^{136}Xe nuclei and producing 1313 keV γ rays. The neutrons from the DD generator will scatter in the xenon both elastically and inelastically. Elastic scatters will tend to deposit small amounts of energy in nuclear recoils, but most neutrons will inelastically scatter or leave the xenon volume before slowing down to an energy below the threshold for inelastic scattering. The monoenergetic 2.5 MeV neutrons from the DD generator are near the optimal energy for the desired inelastic scatter, and are below the thresholds to create undesirable radioisotope contamination through reactions such as ^{63}Cu$(n,\alpha)^{60}$Co. Additionally, the pulsed nature of the generator can be used to isolate prompt inelastic scatters from delayed neutron captures, yielding a cleaner calibration data set.

Using a GEANT4 [27,28] simulation with liquid xenon enriched to 90% ^{136}Xe, we found the effective interaction length for DD generator neutrons to inelastically scatter to be 23 cm. This compares very favorably to γ rays, which have an interaction length below 10 cm. Thus, this could be a useful alternative to external γ sources for calibrating detector response for interactions near the detector center. Calibration using neutron-induced γ rays from activation products or neutron capture is a well-known technique used by experiments such as Super-Kamiokande [29,30]. Additionally, calibration using neutron inelastic scatters has been proposed for nuclear recoil measurements in liquid noble gas detectors [31]. However, we believe that the use of the prompt inelastic scattering γ rays themselves for calibration would be a new technique for detectors designed for electron recoil measurements.

There would be some challenges in implementing this calibration method. The elastic scattering would deposit additional energy in the detector beyond the monoenergetic 1313 keV line. However, these depositions will produce only small amounts of scintillation and ionization (reduced further by quenching), and the position dependence of this could be corrected for via simulations, which do not depend on the detector response, only the neutron propagation physics and quenching factors. The generator would need to be brought near the xenon volume in such a way as to avoid negatively impacting radiopurity during normal running. Neutron captures could likely be excluded from calibration data based on interaction timing, but possible activation or neutron damage to electronics, while unlikely with neutrons below 3 MeV, would need to be considered. Finally, the costs and benefits of this method must be weighed against other techniques for calibrating deep inside detectors, including external γ-ray calibration and dissolving a radioisotope in the xenon volume [32].

VII. DISCUSSION AND SUMMARY

The (n,n') cross sections measured here are similar to estimates from TALYS simulations. The (n,xn) cross sections are not well estimated by TALYS, so this measurement may suggest possible improvements to reaction modeling. All TALYS predictions presented in this work were obtained with the TALYS 1.8 default settings. We have not attempted to test the dependence of the predictions on different models or involved quantities. These measurements, along with newly observed γ lines, may also be used to refine future nuclear evaluations and improve simulations. The measured cross section for the 2415 keV line matches well with recent measurements using $E_n = 2.5$–4.5 MeV made by Peters *et al.* [26]. The E_n dependence of the cross sections for the 1313 keV and 884 keV lines agree within uncertainties with unnormalized measurements from Fotiades *et al.* [33].

We have searched for new γ lines near the ^{136}Xe Q value, and set limits on their possible neutron interaction cross sections for a wide range of E_n. Any lines that may interfere with $0\nu\beta\beta$ measurement have considerably smaller cross sections than the known line at 2415 keV. Next-generation $0\nu\beta\beta$ experiments are designed to have backgrounds near or below a single count per year in the signal region [1]. Our measurement of the cross section of the 1313 keV line could be used to estimate the fast neutron flux, and subsequently set limits on potential fast neutron backgrounds in the $0\nu\beta\beta$ region of interest. Thus, potential fast-neutron-induced backgrounds to $0\nu\beta\beta$ have been well catalogued, and are unlikely to impact future experiments.

The calibration technique proposed here for large liquid noble gas detectors using neutron inelastic scattering to provide a monoenergetic γ ray could be valuable for future experiments. The costs and challenges of this technique will need to be weighed against existing techniques to determine

viability, but, for relevant experiments, it should be worth considering.

ACKNOWLEDGMENTS

This work was funded by U.S. Department of Energy Grant No. DE-SC0012191. This work was performed under the auspices of the U.S. Department of Energy (DOE) under Contract No. DE-AC52-06NA25396. This work has benefited from use of the LANSCE accelerator facility supported under DOE Contract No. DE-AC52-06NA25396. We thank Vladimir Belov for his help studying neutron inelastic scattering as a calibration technique.

[1] S. Al Kharusi *et al.* (nEXO Collaboration), arXiv:1805.11142.
[2] T. Brunner and L. Winslow, Nucl. Phys. News **27**, 14 (2017).
[3] J. B. Albert *et al.* (nEXO Collaboration), Phys. Rev. C **97**, 065503 (2018).
[4] A. Gando, Y. Gando, T. Hachiya, A. Hayashi, S. Hayashida, H. Ikeda, K. Inoue, K. Ishidoshiro, Y. Karino, M. Koga, S. Matsuda, T. Mitsui, K. Nakamura, S. Obara, T. Oura, H. Ozaki, I. Shimizu, Y. Shirahata, J. Shirai, A. Suzuki, T. Takai, K. Tamae, Y. Teraoka, K. Ueshima, H. Watanabe, A. Kozlov, Y. Takemoto, S. Yoshida, K. Fushimi, T. I. Banks, B. E. Berger, B. K. Fujikawa, T. ODonnell, L. A. Winslow, Y. Efremenko, H. J. Karwowski, D. M. Markoff, W. Tornow, J. A. Detwiler, S. Enomoto, and M. P. Decowski, Phys. Rev. Lett. **117**, 082503 (2016).
[5] J. Martín-Albo *et al.* (NEXT Collaboration), J. Phys.: Conf. Ser. **460**, 012010 (2013).
[6] X. Chen *et al.*, Sci. China Phys., Mech. Astron. **60**, 061011 (2017).
[7] M. Redshaw, E. Wingfield, J. McDaniel, and E. G. Myers, Phys. Rev. Lett. **98**, 053003 (2007).
[8] J. B. Albert, S. J. Daugherty, T. N. Johnson, T. OConner, L. J. Kaufman, A. Couture, J. L. Ullmann, and M. Krticka, Phys. Rev. C **94**, 034617 (2016).
[9] P. W. Lisowski, C. D. Bowman, G. J. Russell, and S. A. Wender, Nucl. Sci. Eng. **106**, 208 (1990).
[10] J. A. Becker and R. O. Nelson, Nucl. Phys. News **7**, 11 (1997).
[11] S. Wender, S. Balestrini, A. Brown, R. Haight, C. Laymon, T. Lee, P. Lisowski, W. McCorkle, R. Nelson, W. Parker, and N. Hill, Nucl. Instrum. Meth. A **336**, 226 (1993).
[12] V. E. Guiseppe, M. Devlin, S. R. Elliott, N. Fotiades, A. Hime, D. M. Mei, R. O. Nelson, and D. V. Perepelitsa, Phys. Rev. C **79**, 054604 (2009).
[13] N. Fotiades, G. D. Johns, R. O. Nelson, M. B. Chadwick, M. Devlin, W. S. Wilburn, P. G. Young, J. A. Becker, D. E. Archer, L. A. Bernstein, P. E. Garrett, C. A. McGrath, D. P. McNabb, and W. Younes, Phys. Rev. C **69**, 024601 (2004).
[14] S. MacMullin, Ph.D. thesis, University of North Carolina at Chapel Hill, 2013.
[15] S. MacMullin, M. Boswell, M. Devlin, S. R. Elliott, N. Fotiades, V. E. Guiseppe, R. Henning, T. Kawano, B. H. LaRoque, R. O. Nelson, and J. M. O'Donnell, Phys. Rev. C **85**, 064614 (2012).
[16] R. Beyer *et al.*, Nucl. Phys. A **927**, 41 (2014).
[17] Dietz, Mirco *et al.*, EPJ Web Conf. **146**, 11040 (2017).
[18] D. Radford, Notes on the use of the program gf3, 2000.
[19] N. Fotiades, M. Devlin, R. O. Nelson, and T. Granier Phys. Rev. C **87**, 044336 (2013).
[20] T. Kibédi, T. Burrows, M. Trzhaskovskaya, P. Davidson, and C. Nestor, Nucl. Instrum. Meth. A **589**, 202 (2008).
[21] D. B. Pelowitz, MCNPX User's Manual Version 2.7.0, 2011, LA-CP-11-00438 .
[22] B. Blank *et al.*, Nucl. Instrum. Meth. A **776**, 34 (2015).
[23] A. Sonzogni, Nucl. Data Sheets **95**, 837 (2002).
[24] A. J. Koning, S. Hilaire, and M. C. Duijvestijn, in *Proceedings of the International Conference on Nuclear Data for Science and Technology*, edited by O. Bersillon, F. Gunsing, E. Bauge, R. Jacqmin, and S. Leray (EDP Sciences, Les Ulis, 2008), pp. 211–214.
[25] M. R. Bhat, in *Nuclear Data for Science and Technology*, edited by S. M. Qaim (Springer, Berlin, 1992), pp. 817–821, Data extracted using the NNDC On-Line Data Service from the ENSDF database, file revised as of 5/4/2018.
[26] E. E. Peters, T. J. Ross, S. H. Liu, M. T. McEllistrem, and S. W. Yates, Phys. Rev. C **95**, 014325 (2017).
[27] S. Agostinelli *et al.* (GEANT4), Nucl. Instrum. Meth. A **506**, 250 (2003).
[28] J. Allison *et al.*, IEEE Trans. Nucl. Sci. **53**, 270 (2006).
[29] E. Blaufuss *et al.* (Super-Kamiokande), Nucl. Instrum. Meth. A **458**, 638 (2001).
[30] K. Abe *et al.* (Hyper-Kamiokande), arXiv:1805.04163.
[31] S. Polosatkin, E. Grishnyaev, and A. Dolgov, J. Instrum. **9**, P10017 (2014).
[32] E. Aprile *et al.* (XENON), Phys. Rev. D **95**, 072008 (2017).
[33] N. Fotiades, R. O. Nelson, M. Devlin, J. A. Cizewski, J. A. Becker, W. Younes, R. Krucken, R. M. Clark, P. Fallon, I. Y. Lee, A. O. Macchiavelli, T. Ethvignot, T. Granier, Phys. Rev. C **75**, 054322 (2007).